

Investigation on Microvibration Induced by Reaction Wheels

Mankour Abdeljelil*

Keywords : Microvibration, Reaction wheel, Transfer function, Honeycomb plate

ABSTRACT

Reaction Wheel Assemblies are actuators commonly used for satellite attitude control. During their functioning RWAs produce undesired disturbances transmitted through satellite structure and can significantly affect the performance of vibration-sensitive payload. Microvibrations of a satellite reaction wheel assembly are commonly analysed in either hard-mounted or coupled boundary conditions, though coupled wheel-to-structure disturbance models are more representative of the real environment in which the wheel operates. Micro-vibration is a phenomenon that affects the payload pointing. In this article we want to investigate a solution to damp and decouple the moving part to a soft mounting on the structure that supports the wheels. A couple of core honeycomb plate thickness and mounting stiffness were analyzed to access their damping efficiency on microvibration source. Simulations show that the isolation is effective for micro-vibration suppression and issues about micro-vibration in integrated design are identified.

INTRODUCTION

In the last decades, satellite microvibration and related issues have become a major concern in the design of satellites requiring high stability platforms (Tanguy et al., 2011). They are usually generated by internal mechanisms on board satellites, such as Reaction Wheel Assemblies (RWAs), Momentum Wheel Assemblies (MWAs), cryocoolers, pointing mechanisms, thrusters, ...etc., which in this context are called microvibration sources (Zhang et al. 2009).

The microvibrations caused by such sources are transmitted through the satellite structure, exciting modes of the structure or elements of the instrument

Paper Received September, 2017. Revised January, 2018, Accepted March, 2018, Author for Correspondence: Mankour Abdeljelil.

* Doctor, Department of Mechanical Engineering, Centre of satellite development, Pingtung, Taiwan 91207, ROC.

and affecting its performance (Toyoshima et al. 2003). On the figure below an example of microvibration effect on image quality such distortion.



Fig. 1. Example of micro-vibration effect on geometric distortion (Zhang et al. 2011).

Microvibration on spacecraft is a special kind of vibration which has tiny amplitude and high frequency, whose influence to structure is negligible. However, as to sub-meter satellites, microvibration has become a critical factor for high resolution image quality. With the development of satellite technologies, and the pressing need for high resolution, high agility and low costs, integrated design of satellite platform and payload has been a growing tendency. For earth observation satellites and space telescopes this is becoming an increasingly important requirement due to the development of evermore capable and sensitive optical payloads. Among the various disturbance sources on a spacecraft, RWAs are commonly considered as the largest by (Tanguy et al., 2011 and Miller et al. 2007). The loads are generated due to mass imbalance and local motor bearing imperfections, generated by the RWA when hard-mounted on an isolated and rigid platform. Subsequently, the coupled dynamics when the RWA is assembled with a stiff support (see Figure 3) were measured, in terms of coupled forces at the RWA-structure interface. Even though the reaction wheels are very accurately balanced statically and dynamically, the high speed of operation (≈ 4500 to 5400 RPM), causes dynamic disturbances to the

spacecraft (Davis and al., 1986; Sabins et al., 1976; Fukuda et al., 1986; Bosgra and Prins 1982; NASA Tech. Rep., 1976). The induced disturbances are transferred through the satellite structure towards the payloads and sensitive instruments, exciting their modes of vibration and severely affecting their performance. Moreover, estimates of the microvibration effects become more complicated as the dynamics of the micro-vibration sources also couple with those of the satellite structure (Takahara et al., 2004 and Takahara et al., 2006). In addition, the understanding and control of the vibration level at sensitive locations, using passive damping and active control technologies (Vaillon et al., 2002 and Bae et al., 2012), is also a crucial factor in order to achieve the desired instruments' performance.

To provide good predictions of the satellite performance if the RWA has resonance frequencies well above the frequency range of interest, which is not often the case for microvibration applications; hence the internal dynamics of the source (dynamic mass) need to be taken into account. Many works to investigate and derive the dynamic mass of the source were initially carried out (Elias et al., 2002; Zhang et al., 2012; Zhao et al., 2009). To reduce the influence of micro vibration on imaging, different types of vibration control technologies are used (Liu et al. 2015), namely as passive and active vibration isolations, vibration absorption, vibration resistance, and dynamic designs.

The finite element structure model is the basis of dynamic analysis. The dynamics of a multi-degree-of-freedom system (structure) are described in the time domain by the equation (Lee et al. 2012):

$$\mathbf{M}\ddot{\mathbf{x}} + \mathbf{C}\dot{\mathbf{x}} + \mathbf{K}\mathbf{x} = \mathbf{F}, \quad (1)$$

Where: \mathbf{M} , \mathbf{C} , and \mathbf{K} are $N \times N$ dimensional matrices, of which \mathbf{M} is the mass matrix, \mathbf{C} is the damping matrix, and \mathbf{K} is the stiffness matrix; \mathbf{F} is the force matrix; \mathbf{x} is the displacement response.

A simplified passive isolation system consisting of a mass (m), spring (stiffness coefficient k) and damper (damping coefficient c) with one degree of freedom is shown in Figure 2. Its effective frequency for disturbance isolation is $\sqrt{2}f_n$; where f_n is the natural frequency and is expressed as: $\frac{1}{2}\sqrt{k/m}$. Therefore,

reasonable design of the isolator can be achieved by proper combination design of stiffness and mass. In addition, it can be seen that damping ratio " $\varepsilon(c/2\sqrt{mk})$ " plays an important role in transmissibility. Introducing damping into isolator design could improve isolation performance significantly.

The objective of this work is to determine a key solution for the structure to minimize the transmissibility of microvibrations generated during in orbit operation by moving parts on the spacecraft (e.g. reaction wheels) which may adversely affect sensitive payloads or instruments. We had investigated param-

eters to control the micro-vibration effect. Therefore, the reduction of transfer loads by softening the mounting wheels and modifying the geometry parameters of supporting structure (honeycomb panel).

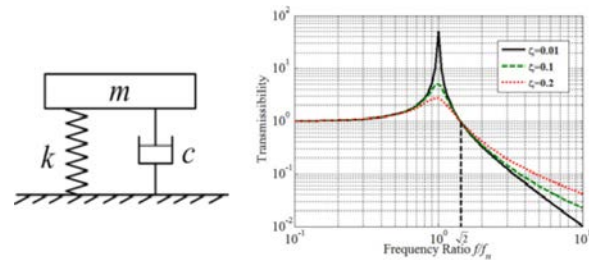


Fig. 2. Passive isolation system and its transmissibility.

MODEL DESCRIPTION

Geometry

Our model is composed of a squared honeycomb plate of (620 × 620 × 20 mm) supporting a reaction wheel (10-SP) in the corner as mentioned in the figure 3; we note that, the wheel is hard mounted on a bracket. The total mass of the wheel is about 1 Kg including the mass of the supporting bracket to the structure.

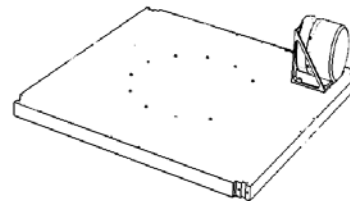


Fig. 3. Reaction wheel hard mounted on the honeycomb plate.

Materials properties

The plate is made of Aluminum (see table 1). In our analysis we used two types of materials Al-2024 T3 and Al5052 for honeycomb panel skin and core respectively and Al-7075 T73 for the inserts properties. The properties of the P-shell card representing the equivalent honeycomb plate are illustrated in table 3. Where: T_c is the core thickness; E_f is the young modulus of face sheet; T_f is the thickness of face sheet; I is the bending moment; NSM is the non-structural mass; μ is the Poisson ratio; g represents the materials density.

Table 1: Materials properties

Materials	Al-2024 T3	Al-7075 T73
Young Modulus E (MPa)	69000	72100
Poison Ratio μ	0.33	0.33
Density g (Kg/m ³)	2768	2796
Shear Modulus (MPa)	25940	27100

Table 2: Orthotropic properties of the honeycomb core

Core material	Al-5052
Density ρ (Kg/m ³)	130
Cell size (m)	0.003
L shear modulus (MPa)	930
W shear modulus (MPa)	372

Table 3: Equivalent properties of P-shell card

T_c (m)	0.0194
T_r (m)	0.0006
E_r (MPa)	70000
μ	0.33
ρ_f (Kg/m ³)	2700
ρ_c (Kg/m ³)	130
I	3136.33
T_c/T_r	32.33
NSM	2.522

Mesh

The results data were measured at the node situated in the center of modeled wheel. The applied force on the COG of the Wheel modeled as a point mass is of magnitude 1 N; the force acted in different directions (X, Y and Z) according to the coordinate system of the plate. We had changed the axial and rotations stiffness “K” of the mounting Wheel which represents the isolation mechanism to analyse the transfer function behaviour of the wheel noise perturbation. Also, we had investigated the role of honeycomb core thickness damping capacity of the transferred loads disturbance to the structure. Hence, the result of force applied on each axis generates three displacements and three rotations (6 DOF).

When building the FEM model, we had used the equivalent P-shell method to model the honeycomb base plate supporting the wheel. Triangular and quadratic elements were used to mesh the plate, the FEM model is composed from 4061 elements and 4172 nodes. A free boundary condition analysis was performed to investigate the displacements and rotations for the six degree of freedom (6DOF) in the center of MPC (Figure 3) node generated from an applied load on the COG of Wheel; the load are applied in the three directions according to coordinate system X,Y and Z.

We had investigated the effect of the plate geometry and damping mechanism to reduce the transferred load perturbation from the wheels to the structure and eventually to the payload. We note that, the wheel is hard mounted to the honeycomb panel. RW is modeled as a point mass in the center of gravity and with the moments of inertia.

Load conditions

The analysis is performed without any constraint (free-free analysis) using MSC NASTRAN.

These boundary conditions simulate the model dynamics in the space environment. Thus, a force is applied on the point mass in each direction (X, Y and Z) of magnitude 1N representing the noise disturbance level produced by the wheel (figure 4). Hence, the displacement output is measured at the center of MPC, in the node ID ‘101562’ on the honeycomb plate to deduce the transfer function from the point masse to the structure.

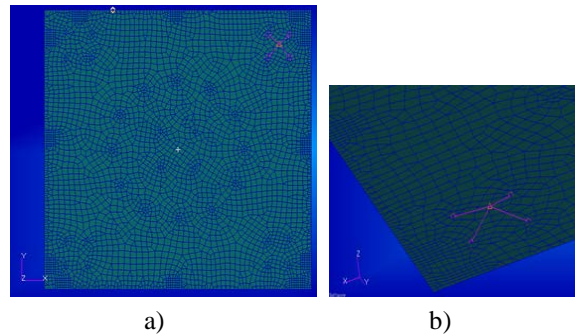


Fig. 4. a) Honeycomb plate supporting the RW b) FE modeling of RW.

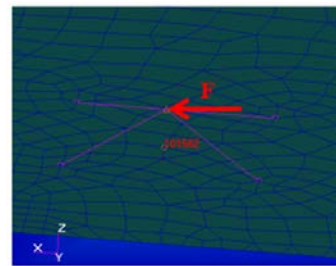


Fig. 5. Location of excitation force towards X direction and node of output measurement ID.

RESULTS AND DISCUSSIONS

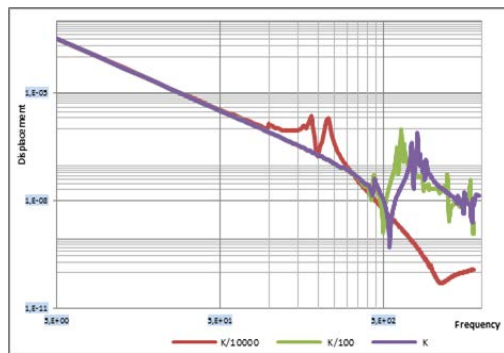
Effect of Wheels mounting stiffness

In the first stage we implement of a damping mechanism for decoupling the resonance modes of wheels and its supporting structure; in order to investigate the behaviour of the transfer function according to the microvibration transmissibility. The connection of the wheel to the structure is modeled by a spring of stiffness K. The figures show the displacements and rotations measured at the node ID (101562) situated in the center of the wheel (modeled as point mass) generated from forces in X, Y and Z directions respectively.

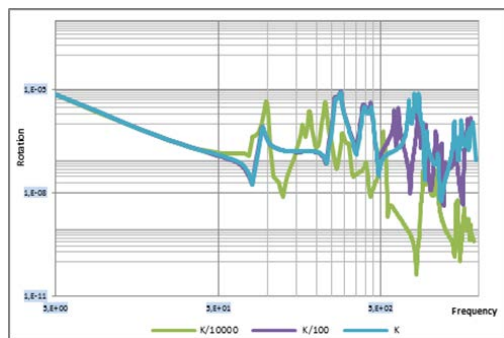
Loading in X direction

In this case, the load is applied in X direction which generates 3 displacements and 3 rotations of the induced node. The figures 6, 7 and 8 represent a comparison of the displacement (Tx) and rotation (Rx) for different wheel mounting stiffness (K). As shown in the figures, the reduction of the mounting stiffness between the wheel and the supporting plate provokes

a reduction of sensitive modes and their amplitudes for all frequency ranges (low, medium and high) for both displacements and rotations.

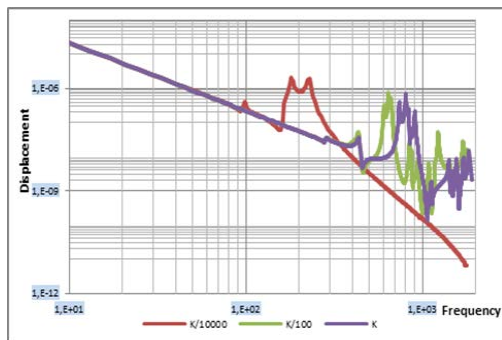


a)

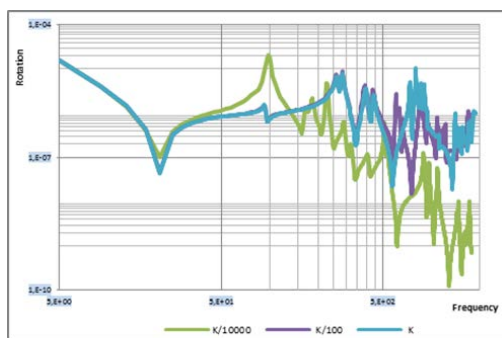


b)

Fig. 6. Translation Tx and rotation Rx vs. Frequency: a) Tx and b) Rx.

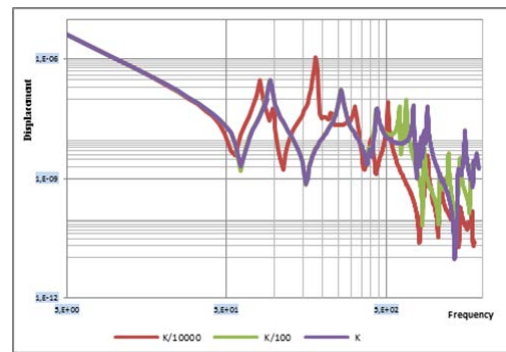


a)

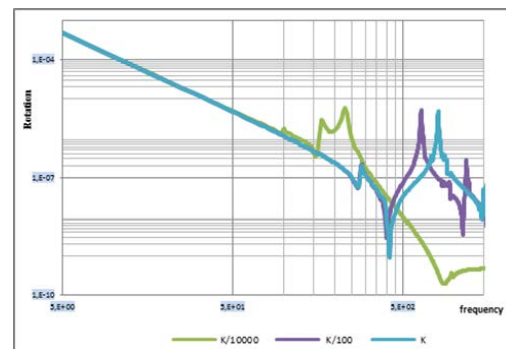


b)

Fig. 7. Translation Ty and rotation Ry vs. Frequency: a) Ty and b) Ry.



a)



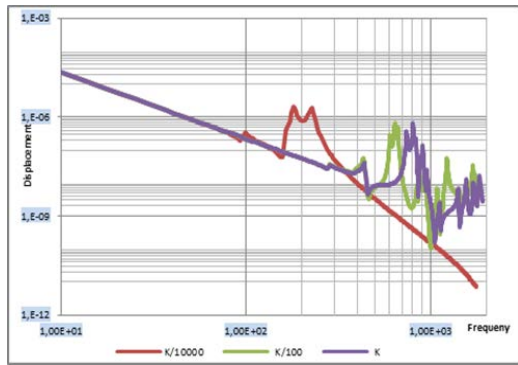
b)

Fig. 8. Translation Tz and rotation Rz vs. Frequency: a) Tz and b) Rz.

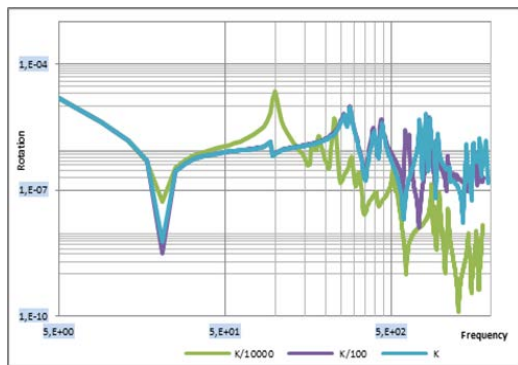
Although, the magnitude of low frequencies increases, contrary to medium and high frequencies which are damped. We note that, the shift amount of the main resonance modes of transfer function is significant for low frequency. we can see in Tx, Ty and Rz that, a significant reduction of the mounting stiffness leads to a bigger amplitude in low frequency range which can gives worst performance results by arising the noise transmissibility to the structure.

Loading in Y direction

The loads applied on the point masse representing the wheel is towards Y direction in this case, the results of dis-placement and rotations are illustrated on figures below for 6 DOF. The figures 9, 10 and 11 illustrate the results of the mounting stiffness the wheel and mounting plate influence on the displacements and rotations. We can see from the figures that, the mounting stiffness reduction affect both, the main mode and its amplitude for displacements and rotations with different amount. Hence, the sensitive modes shift is proportional to the stiffness variation. Also, the major change was observed for low frequency range. Whilst, the amplitudes are higher for low frequencies contrary to medium and high frequency range which are remarkably reduced. We note that, the transfer function of displacements and rotations have almost the same behaviour for X and Y loading case due to the symmetry of the model.

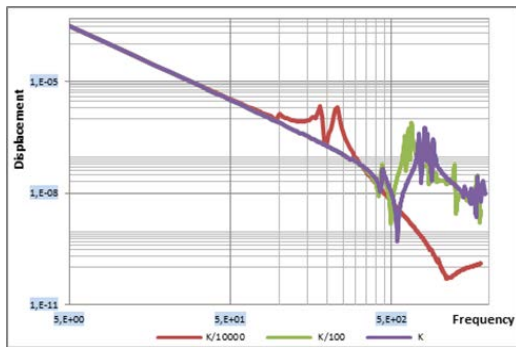


a)

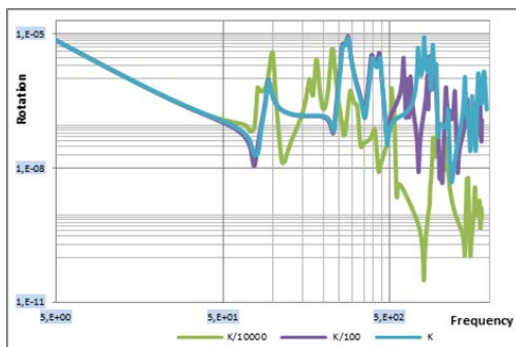


b)

Fig. 9. Translation Tx and rotation Rx vs. Frequency: a) Tx and b) Rx.

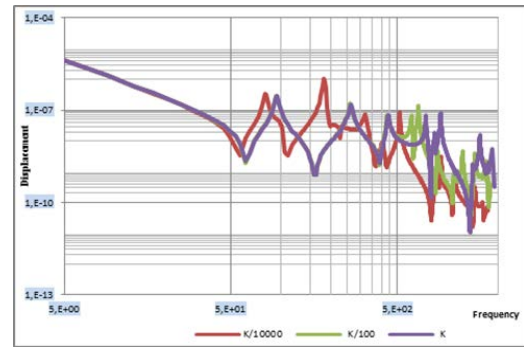


a)

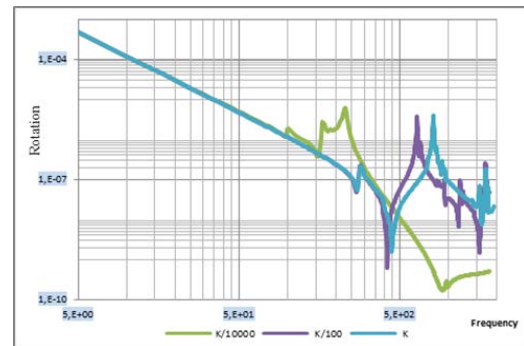


b)

Fig. 10. Translation Ty and rotation Ry vs. Frequency: a) Ty and b) Ry.



a)



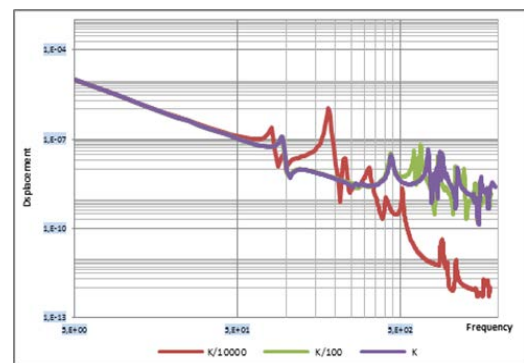
b)

Fig. 11. Translation Tz and rotation Rz vs. Frequency: a) Tz and b) Rz.

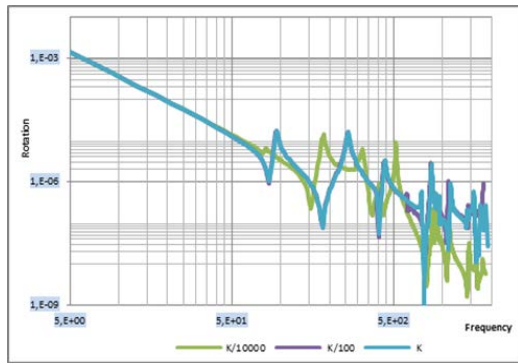
Loading towards Z direction

In this section, the load is applied towards Z direction on the point masse representing the wheel dynamics. The results of displacements and rotations are illustrated on figures 12, 13 and 14 showing the reduction of the mounting stiffness effect for 6 DOF. However, the results are of different magnitude values; since nonlinearity is insignificant in axial translational DOF.

The softening isolation of mounting stiffness induced a shift of sensitive response modes of only high frequencies range. Hence, the decrease of the stiffness by 10000 times induced the changes of sensitive modes which were marked for both displacements and rotations. Besides, if the reduction is consequent, the amplitude of the resonance modes affects all frequency ranges.

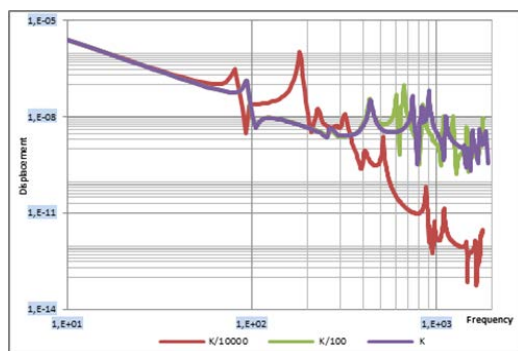


a)

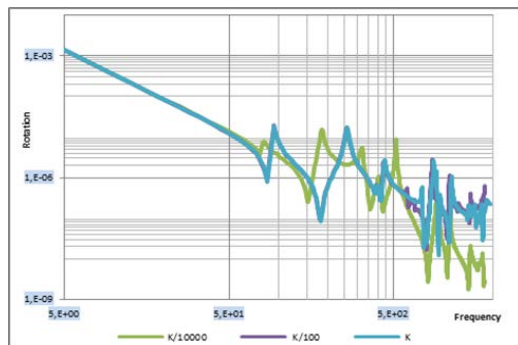


b)

Fig. 12. Translation Tx and rotation Rx vs. Frequency: a) Tx and b) Rx.

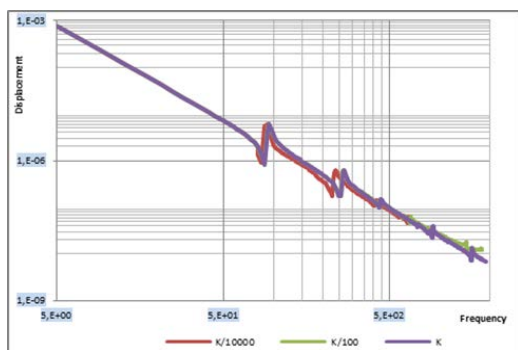


a)

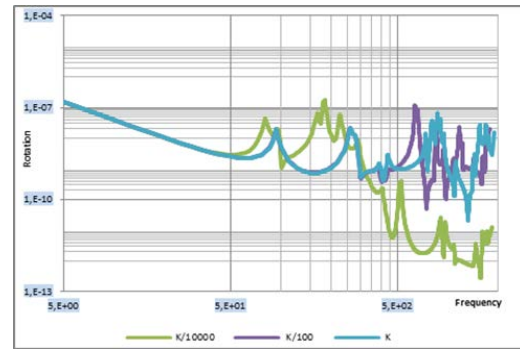


b)

Fig. 13. Translation Ty and rotation Ry vs. Frequency: a) Ty and b) Ry.



a)



b)

Fig. 14. Translation Tz and rotation Rz vs. Frequency: a) Tz and b) Rz.

The insertion of soft mounting can improve the decoupling between the wheel and the structure. Also, the main resonance frequencies modes tend to decrease with higher amplitude for low frequencies and decrease above mid and high frequencies. Furthermore, the effect of the stiffness is more significant for lateral excited directions (X and Y). Also, the softening of the mounting stiffness affects all ranges of frequency response; the low frequency gain in amplitude contrary to medium and high frequency tend to be damped gradually for all direction of load excitation. Furthermore, the reduction of the stiffness leads to decrease the magnitude of the main resonance frequencies. Hence, the hard mounted wheels provoke the medium and high frequencies resonance. Since changes are of significant amount; we can note that, the insertion of a damping system between the wheel bracket and the supporting structure can be an effective solution to control or minimize the disturbance loads transferred from wheels to the structure, and consequently to the payload.

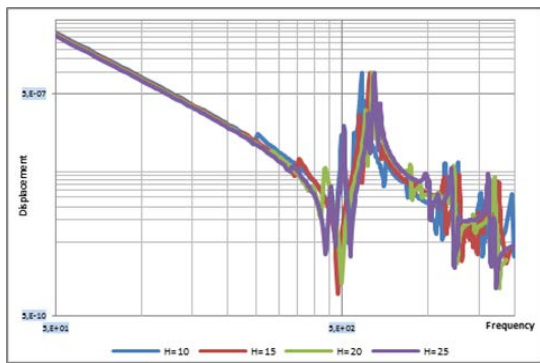
We note that, if the damping ratio is too high, the isolation performance of frequency region could not be satisfied. Therefore, the compromise should be reached between the resonance transmission ratio and isolation performance in low, mid and high frequency region.

Effect of honeycomb panel thickness core analysis

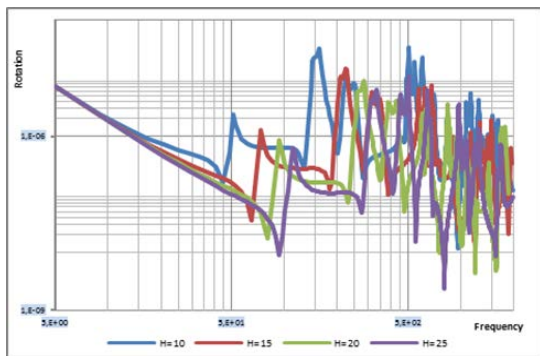
In this section, a set of honeycomb core of thickness 10, 15, 20 and 25 mm was analyzed to investigate the behaviour of transferred loads from the wheel to the supporting structure and eventually to the payload, since the honey-comb plates have a good ability to vibrations absorption.

Loading towards X direction

The figures 15, 16 and 17 presents the transfer function comparison of displacements and rotations according to plate thickness generated from X direction loading for 6 DOF. From the figures results, the thickness of honeycomb plate affects both main sensitive modes and its amplitudes for all ranges frequency (low, medium and high).

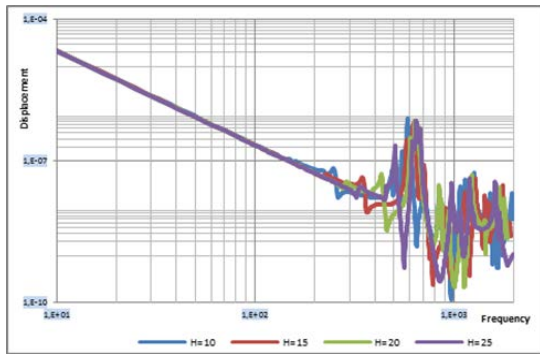


a)

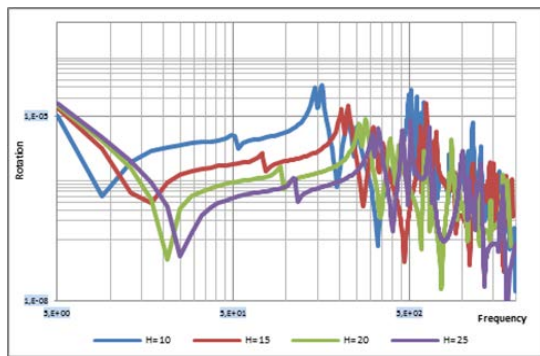


b)

Fig. 15. Translation Tx and rotation Rx vs. Frequency: a) Tx and b) Rx.

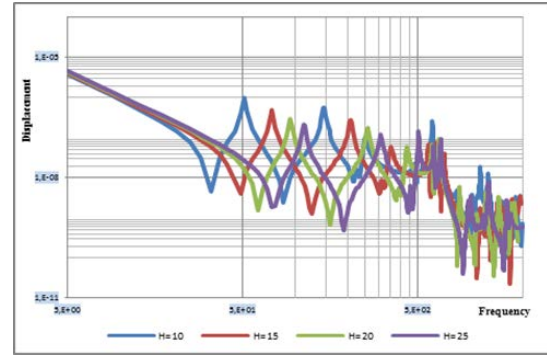


a)

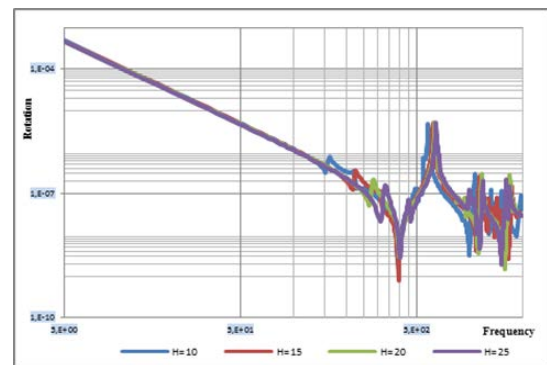


b)

Fig. 16. Translation Ty and rotation Ry vs. Frequency: a) Ty and b) Ry.



a)



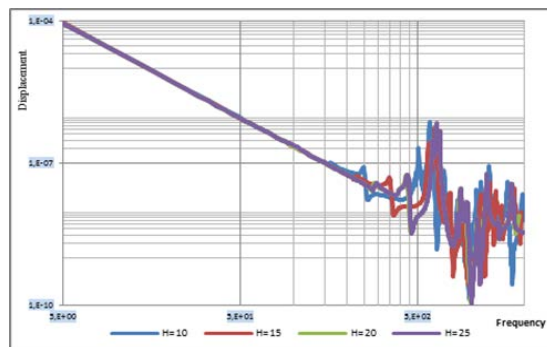
b)

Fig. 17. Translation Tz and rotation Rz vs. Frequency: a) Tz and b) Rz.

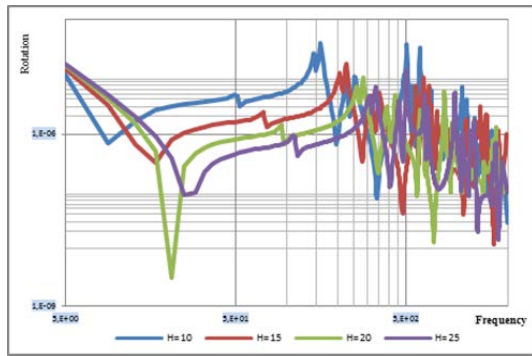
However, the main sensitive modes of the transfer function become bigger with lower amplitude for both displacements and rotations by increasing of the plate thickness respectively. Moreover, the shift of sensitive modes for low frequencies is more important than the others especially for the displacement in Tz direction and rotations Rx and Ry, in addition to its' damping of the transferred loads to the structure.

Loading towards Y direction

The figures 18, 19 and 20 illustrate the comparison of the transfer function of the displacement and rotation in x, y and z according to plate thickness generated from Y loading direction.

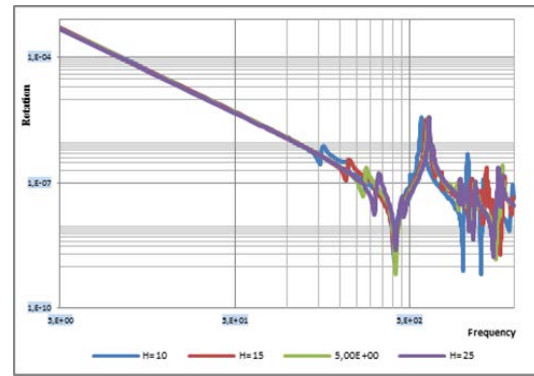


a)



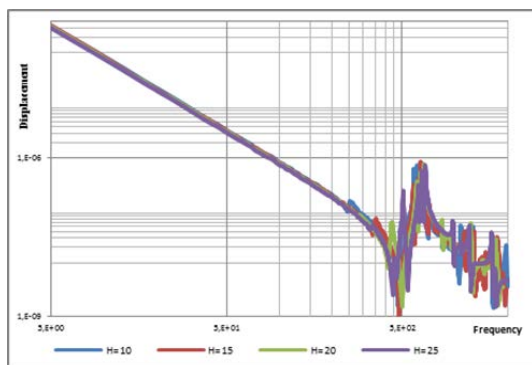
b)

Fig. 18. Translation Tx and rotation Rx vs. Frequency: a) Tx and b) Rx.

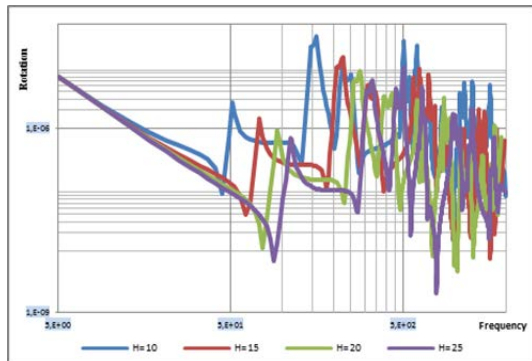


b)

Fig. 20. Translation Tz and rotation Rz vs. Frequency: a) Tz and b) Rz.

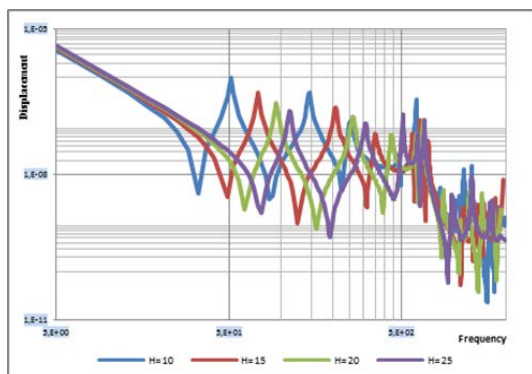


a)

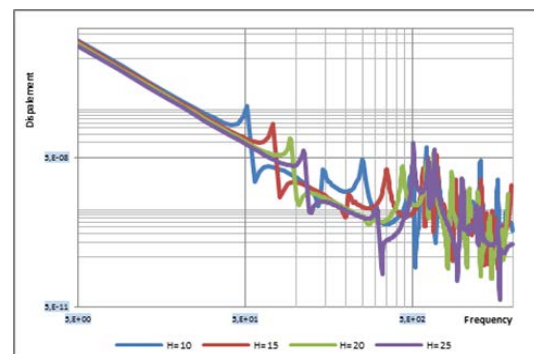


b)

Fig. 19. Translation Ty and rotation Ry vs. Frequency: a) Ty and b) Ry.



a)

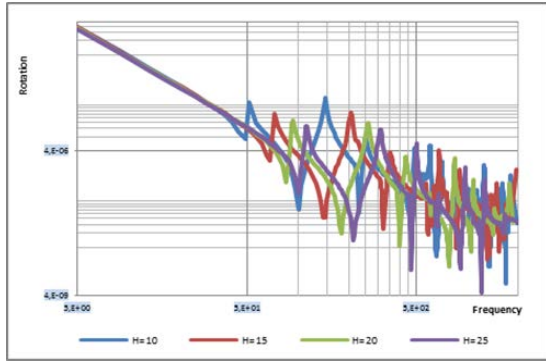


a)

From the results of the figures, the behaviour of the transfer function of displacements T and rotations R towards x, y and z is almost the same due to the symmetry of the structure. However, for all the frequency ranges (low, medium and high) the resonance modes are sifted with different amount, the more important are found for two rotations Rx, Ry and the displacement Tz. Also, the most significant change was observed for low frequencies range followed by decreasing of its amplitude according to the thickness increasing of honeycomb plate.

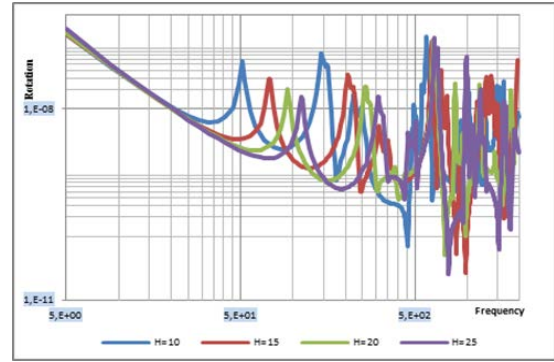
Loading towards Z direction

The figures 21, 22 and 23 illustrate the transfer function variation of the displacements and rotations according to honeycomb plate thickness generated from Z direction loading for 6 DOF's. According the figures results, the resonance amplitude damping and the sensitive modes change is proportional to the core thickness of the plate which is marked by a shift of main modes and the damping of its' amplitude for all displacements and rotations in x, y and z. Thus, the thickness of the core play a major role to damp and decouple and damp the main modes of the transferred load from the hard mounted wheel to the whole structure and consequently to the payload. Thus, all the frequency ranges of rotations and displacements are affected; particularly, the low frequencies resonance modes which are the most affected by the thickness variation.



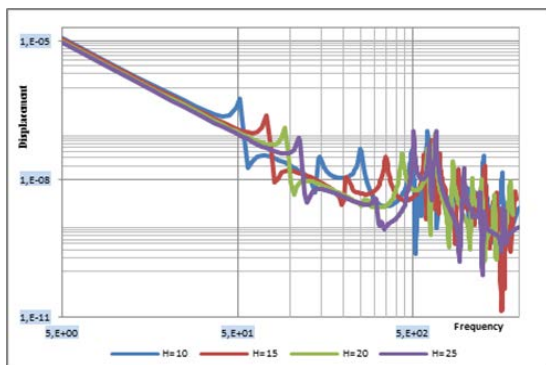
b)

Fig. 21. Translation Tx and rotation Rx vs. Frequency:
a) Tx and b) Rx

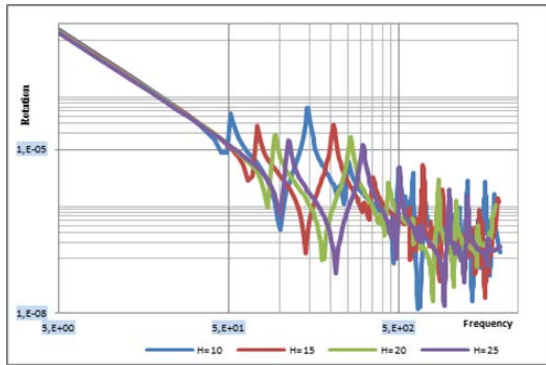


b)

Fig. 23. Translation Tz and rotation Rz vs. Frequency:
a) Tz and b) Rz.

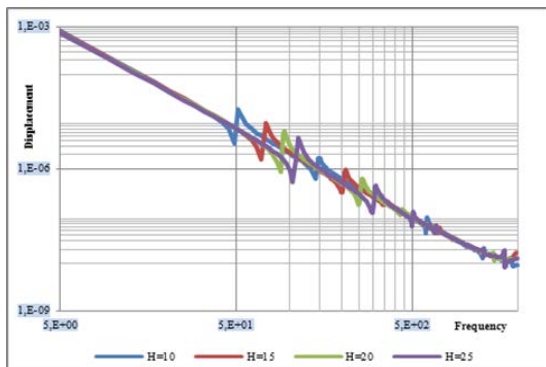


a)



b)

Fig. 22. Translation Ty and rotation Ry vs. Frequency:
a) Ty and b) Ry.



a)

The results comparison of different honeycomb plate thicknesses show an increasing values change for both magnitude and resonance frequency sensitive modes of the transfer function in a proportional behaviour for the three case of loading directions (X, Y and Z). It can be seen that, a shift of frequency resonance modes for low frequency when increasing the thickness of honeycomb core. Furthermore, the effect of honeycomb core is visible for all ranges of frequency (low, medium and high frequency).

Therefore, the thinner plate induces the lower resonance frequencies range, but consequently, it gives higher amplitude for different frequency range; in the other hand, thicker honeycomb plate presents the smallest amplitude for low and medium frequencies. Hence, the disturbance loads generated from the wheel are damped in all load directions (X, Y and Z) for 6 DOF of payload (displacements and rotations).

The size of the main structure, such as the thickness of the plate, can have a significant influence on dynamic parameters of the structure and, then it will affect the transitive property of the micro-vibration. We can deduce that, the honeycomb panel geometrical parameters optimization can be a solution of absorption of the wheels noise disturbance. We note from comparison of the results that, the rate of change ratio in not of significant effect.

CONCLUSIONS

In this article, we investigate a solution to reduce the noise transmission from wheel to the structure. Micro-vibration is a system level problem. It can be handled in many different ways on a spacecraft. Hence, the thickness of honey-comb panel plays a key solution to damp wheels noise transmission to the structure for the hard mounted wheels. Though, we deduce that the insertion of dissipative mechanism is more effective in term of efficiency to decrease the wheels noise disturbance for more stability of the instrument pointing accuracy. So, we can deduce:

- The payload can be designed to be less sen-

sitive to micro-vibration or be mechanically isolated from the rest of the spacecraft as an active attenuation control performance.

- The structure of the spacecraft can be designed to reduce the micro-vibration transmissibility. So, optimal design of layout and configuration is the first choice to reduce the micro-vibration transmitted to sensitive payload.

REFERENCES

- “An evaluation of reaction wheel emitted vibrations for large space telescope”, NASA Technical Report 76N-18213, (Jan 01, 1976).
- Bae J. S., et al. “Vibration suppression of a cantilever beam using magnetically tuned-mass-damper”, *Journal of Sound and Vibration*, 331 (26), pp. 5669–5684 (2012).
- Bosgra, J. A. and Prins, J. J. M., “Testing and investigation of reaction wheels”, *Proceedings of the Ninth IFAC/ESA Symposium, Noordwijkerhout, Netherlands, (July 5-9, 1982).*
- Davis, L. P., Wilson, F., Jewell, R. E., and Roden, J. J., “Hubble space telescope reaction wheel assembly vibration isolation system”, *NASA workshop on structural dynamics and control interaction of flexible structures, GC Marshall Space Flight Center, (March, 1986).*
- Elias, L. M. and Miller, D.W., “A coupled disturbance analysis method using dynamic mass measurement techniques” *Proceedings of the 43rd AIAA/ASME/ASCE/AHS/ASC Structures, Structural Dynamics, and Materials Conference, Denver, Colorado, (April 22-25, 2002).*
- Lee, D. O., Yoon, J. S., and Han, J. H., “Development of integrated simulation tool for jitter analysis” *International Journal of Aeronautical and Space Sciences*, 13(1), pp. 64–73 (2012).
- Liu, C., Jing, X., Daley, S. and Li F., “Recent advances in micro-vibration isolation,” *Mechanical System and Signal Processing*, 56 (1): pp. 55-80 (2015).
- Miller, S.E., Kirchman, P., Sudey, J., “Reaction wheel operational impacts on the goes-n jitter environment” *Proceedings of the AIAA Guidance, Navigation and Control Conference and Exhibit, South Carolina, USA, (August 20-23, 2007).*
- Sabins, S., Schmitt F. and Smith L., “Magnetic reaction wheels”, *NASA Technical Report N76-27336, (1976).*
- Fukuda, T., Hosokai, H. and Yajima, N., “Flexibility control of solar battery arrays”, *Bulletin of the JSME*, 29, pp. 3121-3125, (1986).
- Tanguy, P., Spalinger, E., Shedoni, M. and Guichon, D. “MTG Microvibration Requirements and Associated Potential Impact on the Satellite Design”, *34th Annual Guidance and Control Conference, Breckenridge, CO, (February 4-9, 2011).*
- Toyoshima, M. et al, “Transfer functions of microvibrational disturbances on a satellite”, *Proceedings of the 21st International Communications Satellite Systems Conference and Exhibit, Yokohama, Japan, (15 - 19 April, 2003).*
- Takahara, O., Yoshida, N., Minesugi, K., “Microvibration transmissibility test of solar-b” *Proceedings of the 24th International Symposium on Space Technology and Science, Miyazaki, Japan, (May 30-June 6, 2004).*
- Takahara, O., Ichimoto, K., Kosugi, T., Shimada, S., Yoshida, N., “Evaluation of pointing error for solar-b using optical measurement”, *Uchu Kagaku Gijutsu Rengo Koenkai Koenshu*, 50, pp. 271–275 (2006).
- Vaillon, L., et al, “Flight prototyping of active control of vibration & very high accuracy pointing systems” *Proceedings of the 5th International ESA Conference on Guidance Navigation and Control Systems, Rome, Italy, (October 22-25, 2002).*
- Zhang, Z., Yang, L. and Pang, S. “Jitter environment analysis for micro-precision spacecraft”, *Spacecraft Environment Engineering*, 26 (6), pp. 528–534 (2009).
- Zhang, Z., Remedios, M., Aglietti, G. S., Le page, B. H., Richardson, G., “Methodology of analysis of structure-Borne Micro-vibration” *Internal technical report for ESA and SSTL joint project, ITT No. AO/1-6135/09/NL/NA, (2011).*
- Zhang, Z., Ren, W. and Aglietti, G., “Coupled disturbance modeling and validation of a reaction wheel model” *12th European Conference on Spacecraft Structures, Materials & Environmental Testing, The Netherlands, Noordwijk, (March 20-23, 2012).*
- Zhao, Y., Zhang, P., and Cheng, W. “Measurement and study of disturbance characteristics of reaction wheel assembly” *Journal of Experimental Mechanics*, 24 (6), pp. 532–538 (2009).
- Aurell, J. and Edlund, S., “The Influence of Steered Axles on the Dynamic Stability of Heavy Vehicles,” *SAE paper No. 892498 (1989).*
- Bernard, J.E., Vanderploeg, M.J., and Shannan, J.E, “Linear Analysis of a Vehicle with Four-Wheel

- Steering," *SAE paper* No. 880643 (1988).
- Furleigh, D.D., Vanderploeg, M.J., and Oh, C.Y., "Multiple Steered Axles for Reducing the Rollover Risks of Heavy Articulated Trucks," *SAE paper* No.881866 (1988).
- Kang, X, Rakheja, S. and Stiharu, I., "Effects of Tank Shape on the Roll Dynamic Response of a Partly Filled Tank Vehicle," *Veh. Sys. Dyn.*, Vol.35, No.2, pp.75-102 (2000).
- LeBlane, P.A., El-Gindy, M. and Woodrooffe, J.H.F., "Self-steering axles:Theory and Practice," *SAE paper* No.891633 (1989).
- Rakheja, S., "Roll Plane Analysis of Articulated Tank Vehicles During Steady Turning," *Veh. Sys. Dyn.*, Vol. 17, pp.81-104 (1988).
- Ranganathan, R., Rakheja, S., Sankar, S., "Steady Turning Stability of Partially Filled Tank Vehicles with Arbitrary Tank Geometry," *J. Dyn. Sys. Measur. Contr.*, Vol. 111, No. 3, pp. 481-489 (1989).
- Ranganathan, R., "Influence of Liquid Load Shift on the Dynamic Response of Articulated Tank Vehicles," *Veh. Sys. Dyn.*, Vol.19, pp.177-200 (1990).
- Sano, S., Furukawa, Y. and Shiraishi, S., "Four-Wheel Steering System with Rear Wheel Steer Angle Controlled as a Function of Steering Wheel Angle," *SAE Trans. paper* 860625 (1986).
- Wang, J.Y., *Theory of Ground Vehicles*, John Wiely, New York (1993).
- Wu, D-H, "A Theoretic Study for Yaw/Roll Motions of Multiple Steering Articulated Vehicle," *Pro. I. Mech. Eng. Part D.*, Vol. 215, pp.1257-1265 (2001).
- K Stiffness matrix
- k Stiffness coefficient
- m Mass
- M Mass matrix
- T_c Core thickness
- T_f Thickness of face sheet
- NSM Nonstructural mass
- ε Damping ratio
- μ Poisson ratio

NOMENCLATURE

- c Damping coefficient
- C Damping matrix
- DOF Degree of freedom
- E_f Young modulus of face sheet
- F Force matrix
- f_n Natural frequency
- g Materials density
- I Bending moment of inertia